# Neutron diffraction of hole polaron ordering in $La_{1-x}Sr_xMnO_3$ ($x \simeq \frac{1}{8}$)

Y. Yamada
*Advanced Science Research Center, Japan Atomic Energy Research Institute (JAERI), Tokai, Ibaraki 319-1195, Japan and Advanced Research Center for Science and Engineering, Waseda University, Okubo, Tokyo 169-0072, Japan*

J. Suzuki, K. Oikawa, and S. Katano
*Advanced Science Research Center, Japan Atomic Energy Research Institute (JAERI), Tokai, Ibaraki 319-1195, Japan*

J. A. Fernandez-Baca
*Solid State Division, Oak Ridge National Laboratory (ORNL), Oak Ridge, Tennessee 37831-6393*
(Received 13 October 1999; revised manuscript received 28 February 2000)

The polaron-ordered structure of $La_{1-x}Sr_xMnO_3$ ($x \cong \frac{1}{8}$) has been reinvestigated to verify the previously proposed models. We found satellite reflections on the $(0,k,l)_{ortho}$ and $(1,k,l)_{ortho}$ reciprocal planes. It has been shown that neither of the previously proposed models is completely consistent with the observed results. Based on theoretical consideration of interhole interactions in a perovskite-based structure, the experimental results are analyzed. A polaron ordered structure with unit cell size of $(\sqrt{2}\times\sqrt{2}\times 4)_{cubic}$ has been proposed which is substantially consistent with the observed neutron-scattering pattern.

## I. INTRODUCTION

The mixed valence system expressed by $A_{1-x}B_xMnO_3$ has attracted much attention in recent years because of the abundance of interesting physical properties including a colossal magnetoresistance effect. The variety of phenomena is brought in as the results of interplay between magnetism, transport property, and interaction with lattice of $3d$ electrons/holes on Mn sites. Among these phenomena, charge-hole ordering is quite important because such process directly affects on any macroscopic responses such as resistivity, magnetic and dielectric susceptibilities, elastic constants, etc.

As for highly doped materials in the region $x>0.5$, the charge ordering takes place at sufficiently high temperatures in many substances such as $La_{0.5}Ca_{0.5}MnO_3$, etc., and various important aspects have been elucidated.[1,2] On the other hand, in the case of the materials $x<1/3$, the hole ordering has not been subjected to extensive studies. Yamada *et al.*[3] reported the hole polaron ordering in low-doping rate $La_{1-x}Sr_xMnO_3$ ($x=0.10$ and $0.15$) crystals. Making use of the satellite positions observed in the $(0,k,l)_{ortho}$ reciprocal plane (space group: *Pbnm*), they proposed a hole structure which is consistent with the hole density of $n=\frac{1}{8}$ ($=0.125$), just at the center of $x$ values of the observed specimens. The proposed model structure is reproduced in Fig. 1(a). As is seen in the figure, the holes construct a $2\times2\times4$ unit cell in terms of the cubic perovskite unit.

Recently, Inami *et al.*[4] carried out an x-ray-diffraction experiment using a synchrotron light source on a specimen with $x=0.12$. They proposed an interesting model which is different from the above $(2\times2\times4)_{cubic}$ structure. Based on the observation of the satellites of rather limited numbers, they inferred the extinction rule of the reflections, from which they suggested the new model as given in Fig. 1(b). An important point is that the holes are segregated on every one $(0,0,1)_{ortho}$ layer of successive four layers perpendicular to the orthorhombic $c$ axis where the hole concentration in the hole containing layer is $\overline{n}=\frac{1}{2}$. Moreover, the holes remain disordered in the layer. Thus, the unit cell is $1\times1\times4$ on cubic basis in the averaged sense. The overall hole concentration is $n=\frac{1}{8}$, which is again consistent with the $x$ value of the specimen. While this $(1\times1\times4)_{cubic}$ picture is quite interesting, there arise several questions: Since this is essentially one-dimensional (1D) ordering, is there another phase transition to three-dimensional ordering at a lower temperature? Since the system should be still conductive in the layer, the sharp upturn of resistivity[5] at the onset temperature of 1D ordering seems puzzling. What is the origin of hole segrega-

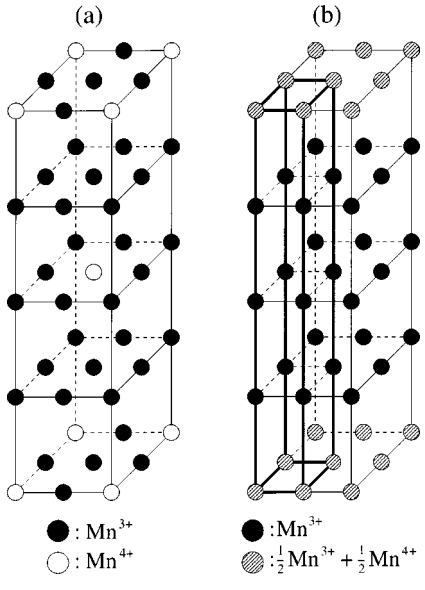


FIG. 1. The previously proposed charge configurations. (a) Proposed by Yamada *et al.*, where the unit cell is $(2\times2\times4)$ in cubic perovskite unit. (b) Proposed by Inami *et al.*, where the unit cell is $(1\times1\times4)$, indicated by the thick lines. In this model, the hole containing layers are spatially segregated.

 ©2000 The American Physical Society

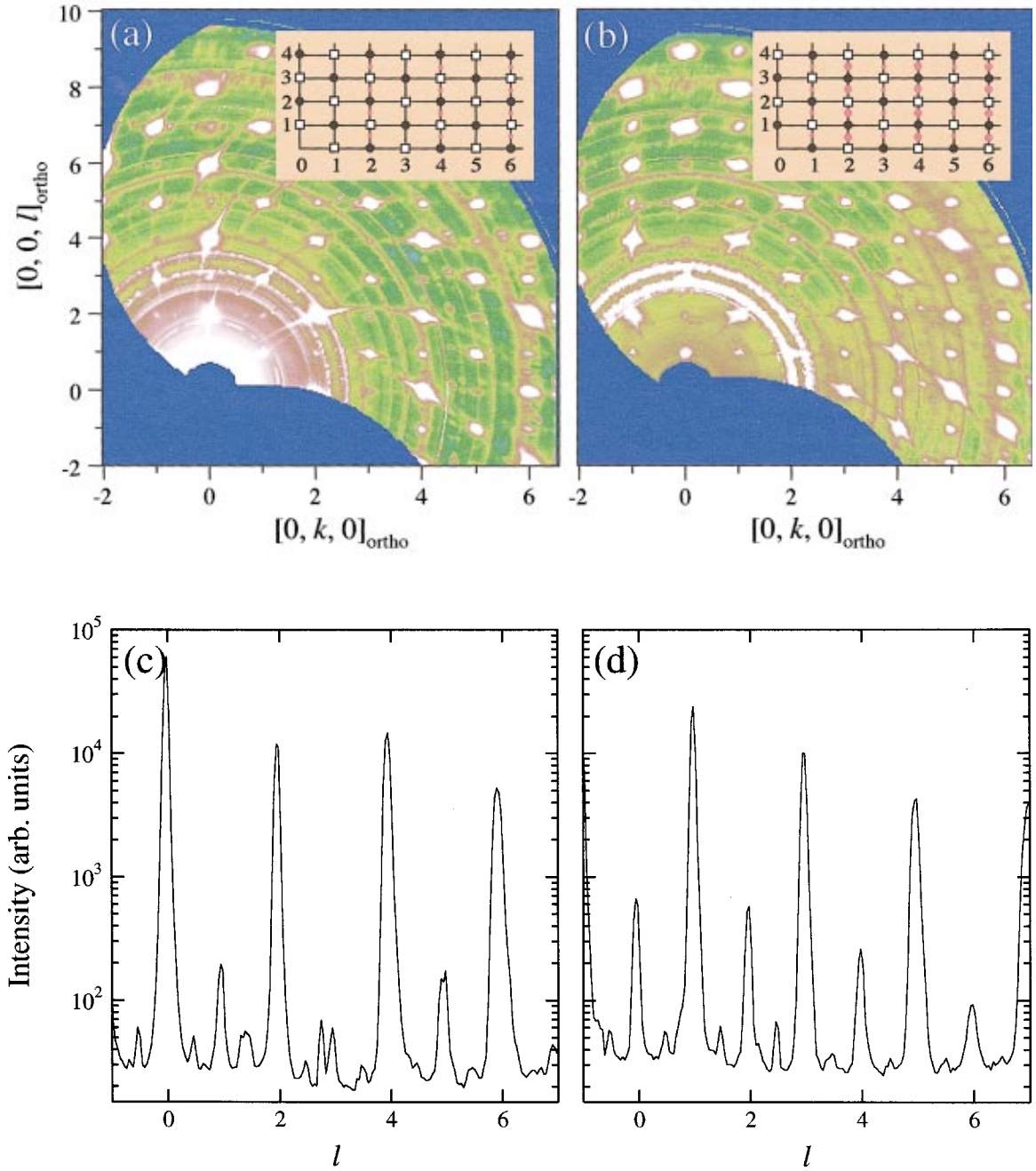


FIG. 2. (Color) The observed neutron-diffraction patterns of (a) $(0,k,l)_{\mathrm{ortho}}$ reciprocal plane and (b) $(1,k,l)_{\mathrm{ortho}}$ reciprocal plane obtained by the WAND diffractometer, installed at the HFIR reactor, ORNL. The inset figures give the corresponding patterns as calculated using Eq. (16) in the text. ●: fundamental reflections due to the basic perovskite structure. □: reflections corresponding to the correct orthorhombic structure belonging to the space group *Pnbm*. Pink solid circles: diffractions due to the polaron ordering. The size of the circles indicates the measure of the relative intensity. The line profiles along $[0,4,l]_{\mathrm{ortho}}$ and $[1,4,l]_{\mathrm{ortho}}$ are also given in (c) and (d), showing weak peaks at $l=2l'\pm\frac{1}{2}$.

tion, which seems energetically unfavorable from electrostatic viewpoint? Moreover, the existence of the orbital order in the same system $La_{1-x}Sr_xMnO_3$ $(x=0.10)$ observed by Endoh *et al.*[6] does not seem to be reconciled with the model. In order to elucidate these points, we have carried out a reinvestigation with neutron-diffraction technique making use of the wide-angle neutron diffractometer[7] (WAND) installed at the high flux isotope reactor (HFIR) of the Oak Ridge National Laboratory (ORNL). The WAND diffractometer enables us to survey wide areas of reciprocal space, so that overall characteristics of the diffraction pattern such as extinction rules are easily obtained. In the next section the experimental procedure and the obtained results are presented. In Sec. III, we describe the framework of the theoretical treatment to discuss the hole-orbital ordered structure, which is utilized for the analysis of the experimental results in Sec. IV. The last section is devoted for summary and discussion.

## II. EXPERIMENTAL PROCEDURES AND RESULTS

A single crystal of $La_{1-x}Sr_xMnO_3$ $(x=0.1)$ used in this study was grown by the floating-zone melting technique. The

dimensions of the sample are 20 mm in length and 4 mm in diameter. The sample is composed of microdomains of the true orthorhombic lattices. The mosaic spread of a single domain is less than 0.8°.

Neutron-diffraction measurements have been carried out using the WAND diffractometer. The wavelength of the incident neutrons is 1.44 Å. The higher-order contaminant from a bent silicon monochrometor working with the (3,1,1) reflection is less than 0.1% compared to the primary beam. The neutrons diffracted by the sample are detected by a curved one-dimensional position-sensitive $^3$He detector, which covers a wide scattering range 125°. We used the flat-cone geometry, one of the Weissenberg methods, to efficiently collect a large number of reflections appearing in the reciprocal planes $(0,k,l)_{\rm ortho}$ and $(1,k,l)_{\rm ortho}$ without any need to remount the sample. The sample was mounted so that it might be rotated around the orthorhombic *a* axis normal to a set of the reciprocal planes. When the reciprocal plane $(0,k,l)_{\rm ortho}$ is observed, the incident beam direction is parallel to the plane. However, in the case of measuring the reciprocal plane $(1,k,l)_{\rm ortho}$ the beam direction is relatively tilted from the reciprocal plane $(0,k,l)_{\rm ortho}$ by about 15°. The sample was cooled down by a standard closed-cycle $^4$He refrigerator.

Figures 2(a) and 2(b) show the diffraction patterns of the reciprocal planes $(0,k,l)_{\rm ortho}$ and $(1,k,l)_{\rm ortho}$ obtained at 12 K, respectively. In both planes we found a series of satellite reflections in addition to the main Bragg reflections $(h,k,l)_{\rm ortho}$ ($h,k,l$: integers). The satellite positions are indexed as $(0,k,l\pm\frac{1}{2})_{\rm ortho}$ and $(1,k,l\pm\frac{1}{2})_{\rm ortho}$ where $k$ and $l$ are even integers. Figures 2(c) and 2(d) show the intensity distribution along $[0,4,l]_{\rm ortho}$ and $[1,4,l]_{\rm ortho}$, respectively, which clearly indicate the systematic presence of satellite reflections. Other reflections observed in both planes, which cannot be indexed systematically probably, come from different domains having slightly different lattice parameters. Furthermore, the rings around the origin and arcs through the main Bragg reflections are the background scatterings from the sample container or the detector.

The satellite reflections appear below $T_p = 110$ K, corresponding to the metal-insulator transition temperature obtained by the resistivity measurement.[5] This result indicates that the polaron ordering due to the freezing of the hole configuration causes the lattice distortion below $T_p$ as previously reported. Within accuracy of experimental resolution, all the observed reflection positions show that the unit cell is given by $\sqrt{2}\times\sqrt{2}\times 4$ in cubic perovskite basis.

## III. THEORETICAL TREATMENT

As is shown in the previous section, rather thorough survey throughout the reciprocal planes $(0,k,l)_{\rm ortho}$ and $(1,k,l)_{\rm ortho}$ by the WAND diffractometer has proven that either of the proposed hole ordered structures, $(2\times2\times4)_{\rm cubic}$ and $(1\times1\times4)_{\rm cubic}$, are inconsistent with the present experimental results (see Appendix A). This seems to suggest that instead of proposing rather arbitrarily constructed model structures, we should carry out some systematic investigation of stabilization process of holes with a fixed density in perovskite-based system.

### A. Hole ordering

There are a number of theoretical works to discuss the charge ordering in $A_{1-x}B_x{\rm MnO_3}$ mainly at the ''half-doped'' ($x=\frac{1}{2}$) condition.[8–10] Since we are only to find the stable charge pattern localized on the Mn site rather than to discuss the overall metal-insulator transition scheme, we simplify the system by taking the narrow band limit of spinless $e_g$ electrons. Then, following the discussion by Lee and Min,[8] the lowest order energy term is given by the intersite Coulombic potential between the holes. For the later convenience, we start with the general expression for the system with $\mu$ sublattices in the unit cell as follows:

$$H=\sum_{\langle i,j\rangle} J_{ij}^{\nu\nu'} S_i^{\nu} S_j^{\nu'} \quad (1\leqslant\nu\leqslant\mu). \tag{1}$$

Here, the pseudospin variable $S_i^{\nu}$ takes on,

$$S_i^{\nu}=\begin{cases}1: & \text{when the } \nu\text{th Mn site in the } i\text{th unit cell is occupied by a hole,}\\ 0: & \text{when it is not occupied by a hole,}\end{cases} \tag{2}$$

and $J_{ij}^{\nu\nu'}$ is the interaction between the pair of holes at $(i,\nu)$ and $(j,\nu')$ sites. In fact, this is an extension of the treatment by Lee and Min[8] to the cases of $x\neq\frac{1}{2}$. By defining the Fourier transforms:

$$S^{\nu}(\mathbf{k})=\frac{1}{\sqrt{N}}\sum_i S_i^{\nu} e^{i\mathbf{k}\cdot\mathbf{r}_i}, \tag{3}$$

$$J^{\nu\nu'}(\mathbf{k})=\frac{1}{\sqrt{N}}\sum_{\langle i,j\rangle} J_{ij}^{\nu\nu'} e^{i\mathbf{k}\cdot\mathbf{r}_{ij}}, \tag{4}$$

the Hamiltonian is expressed as

$$H=\sum_{\mathbf{k}} \mathbf{S}^{+}(-\mathbf{k})\cdot\mathbf{J}(\mathbf{k})\cdot\mathbf{S}(\mathbf{k}). \tag{5}$$

Here, $\mathbf{S}(\mathbf{k})$ is the $\mu$-dimensional column vector,

$$\mathbf{S}(\mathbf{k})=\begin{pmatrix}\mathbf{S}^1(\mathbf{k})\\ \vdots\\ \mathbf{S}^{\mu}(\mathbf{k})\end{pmatrix} \tag{6}$$

and $\mathbf{J}(\mathbf{k})$ is the $(\mu\times\mu)$ matrix given by

$$\mathbf{J}(\mathbf{k})=\begin{pmatrix} \mathbf{J}^{11}(\mathbf{k}) & \mathbf{J}^{12}(\mathbf{k}) & \cdots & \mathbf{J}^{1\mu}(\mathbf{k}) \\ \vdots & & & \vdots \\ \vdots & & & \vdots \\ \mathbf{J}^{\mu 1}(\mathbf{k}) & \cdots & \cdots & \mathbf{J}^{\mu\mu}(\mathbf{k}) \end{pmatrix}. \tag{7}$$

Following the conventional diagonalization procedure, we have

$$H=\sum_{\mathbf{k}}\sum_{\sigma} E^{\sigma}(\mathbf{k})|S^{\sigma}(\mathbf{k})|^2. \tag{8}$$

$E^{\sigma}(\mathbf{k})$ is the energy eigenvalue and $S^{\sigma}(\mathbf{k})$ is the corresponding normal mode specified by the branch index $\sigma$ and the wave vector $\mathbf{k}$. It is reasonable to consider that the stable configuration of holes is given by

$$S_i^{\nu}=C_{\nu}^{\lambda}(\mathbf{k}_0)e^{i\mathbf{k}_0\cdot\mathbf{r}_i}, \tag{9}$$

where $C_{\nu}^{\lambda}(\mathbf{k}_0)$ is the $\nu$th component of the normal coordinate vector $C^{\lambda}(\mathbf{k}_0)$ corresponding to the lowest energy eigenvalue $E^{\lambda}(\mathbf{k}_0)$.

To apply the above consideration to our specific system, we define the pseudocubic (perovskite) unit cell containing single Mn site. Here we have simplified the problem by neglecting anisotropy due to buckling of octahedron in the exact orthorhombic unit cell. We assume that there are two kinds of important interactions to describe the system as follows:

$J_1$: nearest neighbor (NN) interaction in the $(0,0,1)_{\text{cubic}}$ plane,

$J_2$: NN interaction along the $[0,0,1]_{\text{cubic}}$ direction,

where we would reasonably assume as $J_1>J_2>0$ (repulsive interactions).

By solving the one-dimensional seqular equation, it is easy to find the energy eigenvalues as follows:

$$E(\mathbf{k})=2J_1(\cos\mathbf{k}\cdot\mathbf{a}+\cos\mathbf{k}\cdot\mathbf{b})+2J_2\cos\mathbf{k}\cdot\mathbf{c}/2. \tag{10}$$

Clearly, the minimum value of $E(\mathbf{k})$ is at $(\frac{1}{2},\frac{1}{2},\frac{1}{2})_{\text{cubic}}$ (see Fig. 3).

Going back to the real space, the most stable hole density wave (HDW) is expressed as

$$\rho(\mathbf{r})=\overline{\rho}+\delta\hat{\rho}e^{i\mathbf{k}_0\cdot\mathbf{r}},$$
$$\mathbf{k}_0=(\tfrac{1}{2},\tfrac{1}{2},\tfrac{1}{2})_{\text{cubic}}, \tag{11}$$

where $\overline{\rho}$ is the average hole concentration, which is given to be $\overline{\rho}=\frac{1}{8}$ in the present case. Although the amplitude of the modulated part, $\delta\hat{\rho}$, depends on the external condition such as temperature, it is inferred that the maximum value of $\delta\hat{\rho}$ should not exceed $\frac{1}{8}$, because the valence of Mn ions is considered to be fluctuating between $Mn^{3+}$ and $Mn^{4+}$. Finally, the proposed most stable hole configuration [Eq. (11)] is visualized in Fig. 4 taking $\delta\hat{\rho}=\frac{1}{8}$. As is seen in the figure, there are two types of Mn sites aligned along the $[0,0,1]_{\text{cubic}}$ direction: ''hole deficient'' site which is occupied solely by $Mn^{3+}$ ions, and ''hole excess'' site occupied by $Mn^{3.25+}=(\frac{3}{4}Mn^{3+}+\frac{1}{4}Mn^{4+})$. The overall unit cell is specified as $(\sqrt{2}\times\sqrt{2}\times 2)$ on cubic basis.

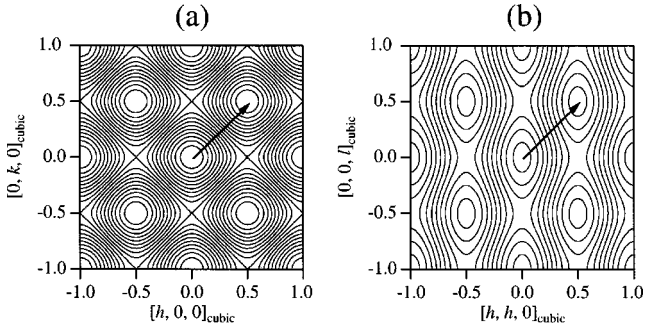


FIG. 3. Energy contour maps of hole density wave state in (a) $(h,k,0)_{\text{cubic}}$ reciprocal plane and in (b) $(h,h,l)_{\text{cubic}}$ reciprocal plane. Notice the lowest energy HDW has the wave vector $\mathbf{k}_0=(\frac{1}{2},\frac{1}{2},\frac{1}{2})_{\text{cubic}}$. The arrows indicate the wave vector of the most stable HDW.

### B. Orbital ordering

At this point, we should notice that due to the degeneracy of the $3d$ orbital in the cubic field, the periodicity of the orbital wave (ORW) does not coincide with the periodicity of the charge-hole density wave. The most frequently observed periodicity of ORW in $A_{1/2}B_{1/2}MnO_3$ ($A$ is La, Nd, $B$ is Sr, Ca) is doubled along the $[1,0,0]_{\text{ortho}}$ direction as compared with that of CDW.[11–13] Since the observed periodicity of the present system is twice of the periodicity of the postulated HDW [Eq. (11)] along the $[0,0,1]_{\text{ortho}}$ direction, we consider that similar situation is also realized in the present case.

In fact, recently Endoh *et al.*[6] clearly observed the evidences of the orbital ordering in the same $La_{1-x}Sr_xMnO_3$ system with $x=0.12$ by resonance x-ray scattering from the $e_g$ electron on $Mn^{3+}$ site at (0,3,0) reflection.

We proceed to find the most stable orbital order under the condition that the hole configuration is fixed by Eq. (11), which forms $(\sqrt{2}\times\sqrt{2}\times 2)_{\text{cubic}}$ lattice. In perovskite manganese oxide $AMnO_3$ system, the wave function of the $e_g$ electron localized on $Mn^{3+}$ site is generally expressed by

$$\phi(\mathbf{r}-\mathbf{r}_{i\kappa})=\frac{1}{2}\varphi_u+\frac{\sqrt{3}}{2}\varphi_{\nu}\tau_i^{\kappa}, \tag{12}$$

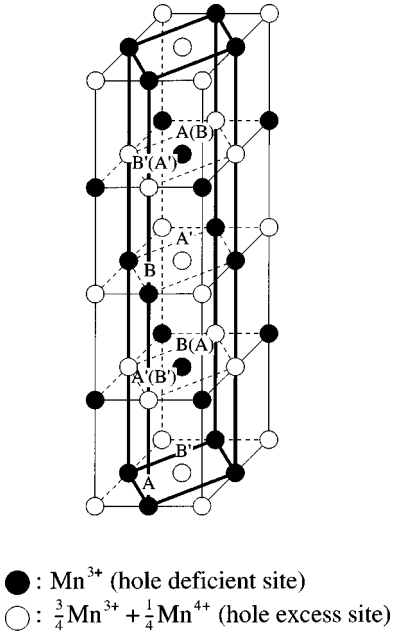


FIG. 4. Proposed hole configuration corresponding to the most stable HDW state as given by Eq. (11). The unit cell of the hole lattice is $(\sqrt{2}\times\sqrt{2}\times 2)_{\rm cubic}$. The most stable ORW (polaron wave) state as given by Eq. (15) is also shown symbolically indicating the local deformation by $A,A',B,B'$. Notice the unit cell of the polaron lattice is $(\sqrt{2}\times\sqrt{2}\times 4)_{\rm cubic}$.

$$\varphi_u(\mathbf{r})\propto 3z^2-r^2,$$

$$\varphi_v(\mathbf{r})\propto x^2-y^2, \tag{13}$$

$$\tau_i^\kappa=\pm 1.$$

Here, $\varphi_u(\mathbf{r})$ and $\varphi_v(\mathbf{r})$ are the well known $3d$ orbitals belonging to the doubly degenerated $E_g$ symmetry of point group $m3m$. The variable $\tau_i^\kappa$ in the second term specifies the orbital elongated in $[1,0,0]_{\rm cubic}$ direction ($\tau_i^\kappa=1$) and $[0,1,0]_{\rm cubic}$ direction ($\tau_i^\kappa=-1$), respectively, at the $\kappa$th site in the $i$th unit cell ($A$ and $B$ in Fig. 5). On the other hand, the orbital state in hole-deficient $Mn^{3.25+}$ site is not exactly known. Recently, the polaronic state of a single $Mn^{4+}$ in pure $LaMnO_3$ has been studied by Allen and Perebeinos.[14] They characterize the state as ''anti-Jahn-Teller'' polaron, which gives similar degenerate orbitals elongated orthogonally ($A'$ and $B'$ in Fig. 4). It would be reasonable to specify the orbital states of $Mn^{3.25+}$ by the same variable $\tau_i^\kappa$. In order to find the stable orbital configuration for the fixed CDW state, we utilize the same theoretical framework previously used to discuss the stable HDW. The ''orbital Hamiltonian'' is given in the same form as Eq. (1) as follows:

$$H'=\sum_{i,j} K_{ij}^{\kappa\kappa}\tau_i^\kappa\tau_j^\kappa, \quad \kappa=(1,2,3,4),$$

$$\tau_i^\kappa=\begin{cases} 1: & \text{when the orbital on } (i,\kappa) \text{ site is elongated along } [1,0,0]_{\rm cubic} \text{ direction,} \\ -1: & \text{when the orbital on } (i,\kappa) \text{ site is elongated along } [0,1,0]_{\rm cubic} \text{ direction,} \end{cases} \tag{14}$$

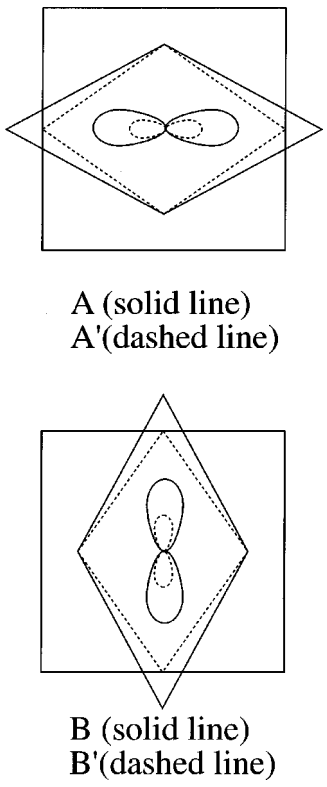


FIG. 5. Schematic representation of the elongated orbitals and the deformation of the oxygen octahedron at various types of small polarons. $A$, $B$ (solid lines): orbital and deformation around the $Mn^{3+}$ site, $A',B'$ (dashed lines): orbital and deformation around the $Mn^{3.25+}$ site. The pattern for $A'(B')$ is taken from Ref. 14.

where $K_{ij}^{\kappa\kappa}$ is the interaction energy between the holes on the $(i,\kappa)$ and $(j,\kappa)$ sites associated with the difference of the orbital configurations.

Again, the present theoretical framework is viewed as a simplified version of the treatment by Ishihara *et al.*[15] in which the freedom of spins is explicitly taken into account in addition to the orbital degree of freedom. Notice there are four sublattices within the orthorhombic unit cell defined for the stable HDW state, $(\sqrt{2}\times\sqrt{2}\times 2)_{\rm cubic}$.

Following the same procedure as the hole ordering, the stable orbital order should be given by the normal mode of the orbital wave $\tau^\lambda(\mathbf{k}_0)$ corresponding to the lowest energy eigenvalue $E^\lambda(\mathbf{k}_0)$, which is explicitly given by solving the eigenvalue equation concerning the $(4\times 4)$ interaction matrix $\{K^{\nu\nu}(\mathbf{k})\}$. As is given in Appendix B in detail, we assume a set of suitable interaction parameters between the neighboring orbitals to define $\{K^{\nu\nu'}(\mathbf{k})\}$, whence to determine the energy eigenstates.

Figure 6 gives the calculated contours of the energy eigenvalues belonging to the lowest energy branch, $E^\lambda(\mathbf{k}_0)$ in $(0,k,l)_{\rm ortho}$ plane. It is seen that the most stable orbital configuration is given by the orbital wave (ORW) state defined by the wave vector $\mathbf{k}_0'=(0,0,\frac{1}{2})_{\rm ortho}=(\frac{1}{2},\frac{1}{2},\frac{1}{4})_{\rm cubic}$. Using Eq. (9), the corresponding stable orbital configuration $\tau_i^\kappa$ is expressed by

$$\tau_i^\kappa=C_\kappa^\lambda(\mathbf{k}_0')e^{i\mathbf{k}_0'\cdot\mathbf{r}}.$$

$$\mathbf{k}_0'=(\tfrac{1}{2},\tfrac{1}{2},\tfrac{1}{4})_{\rm cubic}, \tag{15}$$

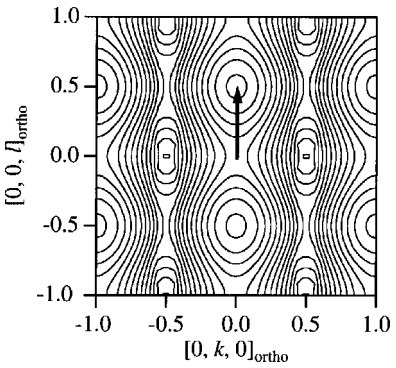


FIG. 6. Energy contour maps of the orbital wave state in the $(0,k,l)_{\text{ortho}}$ reciprocal plane. Notice the lowest energy ORW has the wave vector $\mathbf{k}_0'=(0,0,\frac{1}{2})_{\text{ortho}}=(\frac{1}{2},\frac{1}{2},\frac{1}{4})_{\text{cubic}}$. The arrow indicates the wave vector of the most stable ORW.

where $C_\kappa^\lambda(\mathbf{k}_0')$ is the $\kappa$th component of the eigenvector $C^\lambda(\mathbf{k}_0')$ which is explicitly given by (see Appendix B),

$$C^\lambda(\mathbf{k}_0')=\tfrac{1}{2}(1,-1,e^{i\varphi},-e^{i\varphi}) \tag{16}$$

with arbitrary phase angle $\varphi$. Physically, this means that both sublattices on $z=0$ $(\kappa=1,2)$ and $z_0=\frac{1}{2}$ $(\kappa=3,4)$ (see Fig. 8) stabilize the ''antiferro''-type order while the relative phase relation between them remains indefinite. This is due to that for the ''antiferro''-type order, the orbital configuration on one of the sublattices is frustrated against the other by the translational symmetry of the system.

Finally, the hole-orbital configuration thus determined is depicted in Fig. 4. It is seen that the orbital configuration along the $c$ axis follows the sequence of $A$-$A'(B')$-$B$-$B'(A')\cdots$. Notice due to the frustration, both sequences could be equally probable.

It is noticeable that the present model is consistent with the observation of the orbital order by Endoh *et al.*,[6] since the resonance x-ray structure factor $F(\mathbf{K})$ for $(0,k,l)_{\text{ortho}}$ reflection with ''mixed integer'' such as (0,3,0) is given by $F(\mathbf{K})=\{f_A(\mathbf{K})\text{-}f_{A'}(\mathbf{K})\}+\{f_B(\mathbf{K})\text{-}f_{B'}(\mathbf{K})\}\neq 0$, where $f_A(\mathbf{K})$, etc. is the resonance scattering amplitude for the Mn ion in ''$A$'' configuration, etc. in Fig. 4.

## IV. ANALYSIS OF NEUTRON SPECTRA

So far, we have only considered the ordering of the ''bare'' holes. Actually, the holes should be dressed by local distortion of oxygen to form small polarons. In fact, neutron wave probes only atomic distortions rather than the density of $3d$ electrons (holes) itself.

The local lattice distortion associated with the HDW and ORW is considered to be composed of the following two components:

(i) ''breathing'' mode induced by deficiency-excess of holes relative to $\overline{\rho}$, which belongs to totally symmetric $A_{1g}$ representation of point group $m3m$.

(ii) ''JT active mode'' induced by the Jahn-Teller and anti–Jahn-Teller coupling, which belong to the $E_g$ representation.

In order to define the displacement field throughout the crystal, we adopt the ''half-oxygen model,'' which assumes that there are six independent ''half-oxygens'' octahedrally

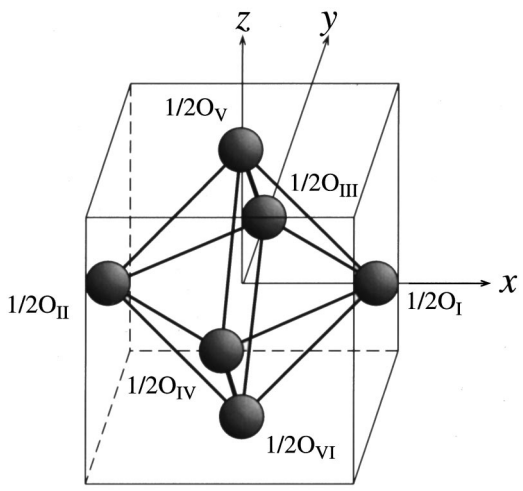


FIG. 7. The arrangement of ''half-oxygen'' ions in the lattice. There are six independent half-oxygens within the cubic perovskite unit cell.

surrounding each Mn ion in perovskite unit cell (Fig. 7). Then, the displacement field associated with the HDW and the ORW is expressed in terms of the two lattice distortion waves (LDW) as follows:

$$\begin{aligned}
&\mathbf{u}^{(\nu)}=\mathbf{u}_A^{(\nu)}e^{i\mathbf{k}_0\cdot\mathbf{r}_i}+\mathbf{u}_E^{(\nu)}e^{i\mathbf{k}_0'\cdot\mathbf{r}_i} \quad (\nu=1,...,6),\\
&\mathbf{u}_A^{(\nu)}=\varepsilon\mathbf{e}_A^{(\nu)},\\
&\mathbf{u}_E^{(\nu)}=\delta\mathbf{e}_E^{(\nu)},
\end{aligned} \tag{17}$$

where $\mathbf{e}_A^{(\nu)}$ and $\mathbf{e}_E^{(\nu)}$ are the $\nu$th components of the normal coordinates of the local $A_{1g}$ mode and of $E_g$ mode, respectively (see Table I).

Finally, the total displacement field is given, by taking into account the ''buckling mode'' which already exists in the original orthorhombic structure, as follows:

$$\begin{aligned}
&\mathbf{u}_i^{(\nu)}=\mathbf{u}_A^{(\nu)}e^{i\mathbf{k}_0\cdot\mathbf{r}_i}+\mathbf{u}_E^{(\nu)}e^{i\mathbf{k}_0'\cdot\mathbf{r}_i}+\mathbf{u}_T^{(\nu)}e^{i\mathbf{k}_0\cdot\mathbf{r}_i} \quad (\nu=1,...,6),\\
&\mathbf{u}_T^{(\nu)}=\phi\mathbf{e}_T^{(\nu)},
\end{aligned} \tag{18}$$

TABLE I. The local displacement of half oxygens in the hole ordered phase. $\mathbf{u}_A^{(\nu)}$ is the displacement of the $\nu$th $\frac{1}{2}$O associated with the hole density order belonging to $A_{1g}$ representation. $\mathbf{u}_E^{(\nu)}$ is the displacement of the $\nu$th $\frac{1}{2}$O associated with the orbital order belonging to $E_g$ representation. $\mathbf{u}_T^{(\nu)}$ is the displacement of the $\nu$th $\frac{1}{2}$O due to tilting of $\frac{1}{2}O_6$ octahedron which already exists in the orthorhombic structure in the disordered state.

| $\nu$ | $\mathbf{r}^{(\nu)}$ | $\mathbf{u}_A^{(\nu)}$ | $\mathbf{u}_E^{(\nu)}$ | $\mathbf{u}_T^{(\nu)}$ |
|---|---|---|---|---|
| 1 | $(\frac{1}{2},0,0)$ | $(\varepsilon,0,0)$ | $(\delta,0,0)$ | $(0,0,\phi)$ |
| 2 | $(-\frac{1}{2},0,0)$ | $(-\varepsilon,0,0)$ | $(-\delta,0,0)$ | $(0,0,-\phi)$ |
| 3 | $(0,\frac{1}{2},0)$ | $(0,\varepsilon,0)$ | $(0,-\delta,0)$ | $(0,0,\phi)$ |
| 4 | $(0,-\frac{1}{2},0)$ | $(0,-\varepsilon,0)$ | $(0,\delta,0)$ | $(0,0,-\phi)$ |
| 5 | $(0,0,\frac{1}{2})$ | $(0,0,\varepsilon)$ | $(0,0,0)$ | $(-\phi,-\phi,0)$ |
| 6 | $(0,0,-\frac{1}{2})$ | $(0,0,-\varepsilon)$ | $(0,0,0)$ | $(\phi,\phi,0)$ |

TABLE II. Calculated structure factors for the satellite reflections at $(h,k,2l'\pm\frac{1}{2})_{\rm ortho}$ within $(0,k,l)_{\rm ortho}$ and $(1,k,l)_{\rm ortho}$ reciprocal planes.

| $h$ | $k$ | $F_E(\mathbf{K})$ | $F_{EA}(\mathbf{K})$ | $F_{ET}(\mathbf{K})$ | $F(\mathbf{K})$ |
|---|---|---|---|---|---|
| $h=0$ | $k=2k'$ | | 0 | $(-1)^{k'+1}8b\pi^2$ $\times(l'+\frac{1}{4})k'\delta\phi$ | $(-1)^{k'+1}8b\pi^2$ $\times(l'+\frac{1}{4})k'\delta\phi$ |
| | $k=2k'+1$ | 0 | | | 0 |
| $h=1$ | $k=2k'$ | $(-1)^{k'+1}4ib\pi^2$ $\times k'\delta$ | | | $(-1)^{k'+1}4ib\pi^2$ $\times k'\delta$ |
| | $k=2k'+1$ | | $(-1)^{k'}4b\pi^2$ $\times(2k'^2+2k'+1)\delta\varepsilon$ | $(-1)^{k'}4b\pi^2$ $\times(l'+\frac{1}{4})\delta\phi$ | $(-1)^{k'}4b\pi^2$ $\times\delta\{(2k'^2+2k'+1)\varepsilon+(l'+\frac{1}{4})\phi\}$ |

where $\mathbf{e}_T^{(\nu)}$ is the $\nu$th component of the normal coordinate of the local tilting deformation (see Ref. 3). The values of $\mathbf{u}_A^{(\nu)}$, $\mathbf{u}_E^{(\nu)}$, and $\mathbf{u}_T^{(\nu)}$ are listed in Table I including disposable parameters $\varepsilon$, $\delta$, and $\phi$.

The structure factor $F(\mathbf{K})$ of neutron scattering associated with the half-oxygens is given by

$$F(\mathbf{K})=\frac{b}{2}\sum_i\sum_{\nu=1}^{6} e^{i\mathbf{K}\cdot(\mathbf{r}_i+\mathbf{r}^{(\nu)}+\mathbf{u}_i^{(\nu)})}, \tag{19}$$

where $b/2$ is the neutron-scattering length of a half-oxygen. In particular, the structure factors for the satellite reflections are expressed by expanding $F(\mathbf{K})$ with respect to $\mathbf{K}\cdot\mathbf{u}_i^{(\nu)}$, by

$$F(\mathbf{K})=F_E(\mathbf{K})+E_{EA}(\mathbf{K})+F_{ET}(\mathbf{K}), \tag{20}$$

$$F_E(\mathbf{K})=\frac{b}{2}\sum_\nu (i\mathbf{K}\cdot\mathbf{u}_E^{(\nu)})e^{i\mathbf{K}\cdot\mathbf{r}^{(\nu)}}\delta(\mathbf{K}-\mathbf{K}_h\pm\mathbf{k}_0), \tag{21}$$

$$F_{EA}(\mathbf{K})=\frac{b}{2}\sum_\nu (i\mathbf{K}\cdot\mathbf{u}_E^{(\nu)})(i\mathbf{K}\cdot\mathbf{u}_A^{(\nu)}) \times e^{i\mathbf{K}\cdot\mathbf{r}^{(\nu)}}\delta(\mathbf{K}-\mathbf{K}_h\pm\mathbf{k}_0\pm\mathbf{k}_0'), \tag{22}$$

$$F_{ET}(\mathbf{K})=\frac{b}{2}\sum_\nu (i\mathbf{K}\cdot\mathbf{u}_E^{(\nu)})(i\mathbf{K}\cdot\mathbf{u}_T^{(\nu)})e^{i\mathbf{k}\cdot\mathbf{r}^{(\nu)}} \times\delta(\mathbf{K}-\mathbf{K}_h\pm\mathbf{k}_0\pm\mathbf{k}_0'), \tag{23}$$

where $\mathbf{K}_h$ is a cubic reciprocal lattice point. $F_E(\mathbf{K})$ peaks at $\mathbf{K}=\mathbf{K}_h\pm(\frac{1}{2},\frac{1}{2},\frac{1}{4})_{\rm cubic}$, while $F_{EA}(\mathbf{K})$ and $F_{ET}(\mathbf{K})$ give peaks at $\mathbf{K}=\mathbf{K}_h\pm(0,0,\frac{1}{4})_{\rm cubic}$. Notice that $F_E(\mathbf{K})$ is the major diffraction effect, while $F_{EA}(\mathbf{K})$ and $F_{ET}(\mathbf{K})$ originate from the second-order terms in the expansion series of $F_E(\mathbf{K})$ with respect to $\mathbf{K}\cdot\mathbf{u}_i^{(\nu)}$. The result of the calculation of $F(\mathbf{K})$ at the satellite positions within $(0,k,l)_{\rm ortho}$ and $(1,k,l)_{\rm ortho}$ reciprocal planes is summarized in Table II. It is easily seen that the major contributions are at $(1,k,2l'\pm\frac{1}{2})_{\rm ortho}$ with $k$ even. In $(0,k,l)_{\rm ortho}$ reciprocal plane, only minor intensities are present at $(0,k,2l'\pm\frac{1}{2})_{\rm ortho}$ with $k$ even. These features are consistent with the observed results. However, there are additional minor intensities at $(1,k,2l'\pm\frac{1}{2})_{\rm ortho}$ with $k$ odd, which is absent in the observed diffraction pattern. This discrepancy has been left unclarified. These overall features are visualized by the insets of Figs. 2(a) and 2(b).

## V. SUMMARY AND DISCUSSIONS

We investigated the structure of $La_{1-x}Sr_xMnO_3$ ($x=0.1$) in order to verify the proposed models of polaron ordering using the WAND diffractometer installed at the HFIR reactor. We found satellite reflections on $(0,k,l)_{\rm ortho}$ and $(1,k,l)_{\rm ortho}$ reciprocal planes. It has been shown that either of the previous models is not completely consistent with the observed results. Based on theoretical consideration of interhole and interorbital interactions in the perovskite-based crystal structure, the experimental results are analyzed. A new polaron ordered structure has been proposed which is substantially consistent with the observed neutron-scattering pattern.

In the present treatment, we have adopted the ''half-oxygen model,'' which inevitably introduces extra fictitious freedom of motion for each oxygen ion. To be more realistic, we should expand the displacement field of oxygen ions in terms of the phonon modes, rather than the local modes, of the perovskite system containing three oxygens in the cubic unit cell. The expression of $\mathbf{u}_i^{(\nu)}$ in Eq. (18) should then be replaced by

$$\mathbf{u}_i^{(\nu)}=\sum_s Q_s(\mathbf{q}_0)\mathbf{e}_\nu^s(\mathbf{q}_0)\exp(i\mathbf{q}_0\cdot\mathbf{r}_i^{(\nu)}) \quad (\nu=1,2,3), \tag{24}$$
$$\mathbf{q}_0=(\tfrac{1}{2},\tfrac{1}{2},\tfrac{1}{4})_{\rm cubic},$$

where $Q_s(\mathbf{q}_0)$ is the amplitude of the phonon mode belonging to the $s$th branch and $\mathbf{e}_\nu^s(\mathbf{q}_0)$ is the normal coordinate of the $\nu$th oxygen. It would be important to investigate lattice dynamical properties extensively in order to elucidate the orbital ordering in this material more precisely beyond the ''half-oxygen'' model.

It is interesting to notice that, while the charge pattern within the $(0,0,1)_{\rm ortho}$ basal plane is essentially the same as the charge pattern commonly found in materials generally expressed as $A_{1/2}B_{1/2}MnO_3$ ($A$ is La, Pr, Nd, $B$ is Sr, Ca),[11–13] the orbital order in $La_{7/8}Sr_{1/8}MnO_3$ and those in $A_{1/2}B_{1/2}MnO_3$ are quite different: In the former, the orbital unit cell is doubled along the $[0,0,1]_{\rm ortho}$ direction, while in the latter, it is doubled along the $[1,0,0]_{\rm ortho}$ direction.

Within the framework of the present treatment, the difference is explained by assuming slightly different set of the $K$ parameters. It would be interesting to estimate these parameters from a microscopic viewpoint for the systems with different $x$ values.


## ACKNOWLEDGMENTS

The neutron-diffraction experiments were carried out at the Oak Ridge National Laboratory under the U.S.-Japan cooperative program on neutron scattering. Oak Ridge National Laboratory is managed by UT-Battelle, LLC, for the U.S. Department of Energy under Contract No. DE-AC05-00OR22725.


## APPENDIX A

The observed satellite pattern seems to be in contradiction to the previous models. In the Yamada model, the translational symmetry of the CDW itself is different from the lattice deduced from the observed satellite positions. On the other hand, in the Inami model, the translational symmetry is correctly defined to give $(\sqrt{2}\times\sqrt{2}\times 4)_{\rm cubic}$. However, the calculation of the structure factors shows that the extinction rule predicted by the model is in disagreement with the observed systematic appearance of the satellites in $(1,k,l)_{\rm ortho}$ plane as shown below.

In the Inami model, the holes are randomly distributed within each segregated ''hole-containing layer.'' Accordingly the effect of the hole ordering is completely wiped out within the layer on average. The only possible structural effect should be the modulation of the spacing of $(0,0,1)_{\rm ortho}$-atomic planes along the $c$ axis.

The displacement field of the ions in the crystal is expressed by

$$\mathbf{u}_i^{\nu}=\hat{\mathbf{u}}e^{i\mathbf{k}_0\cdot\mathbf{r}_i^{\nu}}+\text{c.c.},$$

$$\mathbf{k}_0=(0,0,\tfrac{1}{2})_{\rm ortho}, \tag{A1}$$

$$\hat{\mathbf{u}}\|[0,0,1],$$

where $i$ runs over all unit cells in terms of the exact orthorhombic lattice and $\nu$ specifies the atomic positions in the orthorhombic unit cell.

The structure factor of the neutron scattering, which directly probes the displacement field, is given by

$$F(\mathbf{K})=\sum_{i,\nu} b_{\nu}e^{i\mathbf{K}\cdot(\mathbf{r}_{0,i}^{\nu}+\mathbf{u}_i^{\nu})}=F_0(\mathbf{K})\,\delta(\mathbf{K}-\mathbf{K}_h)$$

$$+i(\mathbf{K}\cdot\hat{\mathbf{u}})\sum_{\nu} b_{\nu}e^{i\mathbf{K}\cdot\mathbf{r}_0^{\nu}}\delta(\mathbf{K}-\mathbf{K}_h\pm\mathbf{k}_0), \tag{A2}$$

$$\mathbf{K}_h=h\mathbf{a}_0^*+k\mathbf{b}_0^*+l\mathbf{c}_0^*.$$

The first term gives the ordinary Bragg peaks at the orthorhombic reciprocal-lattice points. The second term gives the new reflections at $(h,k,2l\pm\frac{1}{2})_{\rm ortho}$, which coincides exactly to the observed satellite positions.

However, detailed calculation of the structure factors of the satellite gives the following systematic rule:

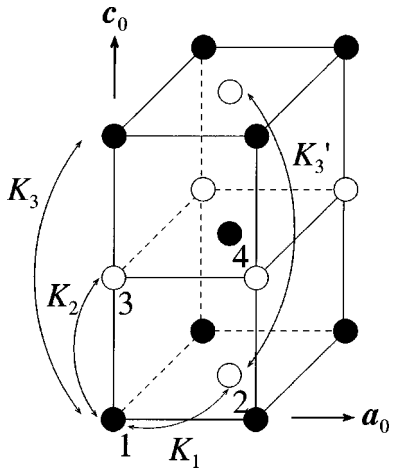


FIG. 8. The energy parameters associated with the orbital states on the sublattices $\kappa=1,2,3,4$, in the $(\sqrt{2}\times\sqrt{2}\times 2)_{\rm cubic}$ hole ordered unit cell.

$$F(\mathbf{K})=(2l\pm 1)\hat{\mathbf{u}}\overline{F}(\mathbf{K}),\quad h+k\ \text{ even}$$

$$=0,\quad h+k\quad \text{odd}, \tag{A3}$$

where $\overline{F}(\mathbf{K})$ is the layer structure factor of the Mn-containing layer.

While the observed satellites on $(0,k,l)_{\rm ortho}$ plane satisfy the above extinction rule, those on the $(1,k,l)_{\rm ortho}$ plane are completely in contradiction since the observed satellites systematically appear at $(1,k,2l\pm\frac{1}{2})_{\rm ortho}$ with $k$ even. This situation seems to rule out the Inami model.

## APPENDIX B

We take into account four important interactions associated with the orbital configuration as follows (see Fig. 8) $K_1$ is the interaction between the nearest-neighbor $Mn^{3+}$-$Mn^{3.25+}$ pairs in the $(0,0,1)_{\rm ortho}$ plane, $K_2$ is the interaction between the nearest-neighbor $Mn^{3+}$-$Mn^{3.25+}$ pairs along the $[0,0,1]_{\rm ortho}$ axis, $K_3$ is the interaction between the next-nearest-neighbor $Mn^{3+}$-$Mn^{3+}$ pairs along the $[0,0,1]_{\rm ortho}$ axis, $K_3'$ is the interaction between the next-nearest-neighbor $Mn^{3.25+}$-$Mn^{3.25+}$ pairs along the $[0,0,1]_{\rm ortho}$ axis. Here, we take $K_1>0$ (antiferro coupling) by considering the well-known in-plane orbital ordering in pure $LaMnO_3$. $K_3$, $K_3'$ are also assumed as $K_3$, $K_3'>0$. $K_2$ can be taken arbitrary as is shown later. The matrix elements of $\{K^{\kappa\kappa}(\mathbf{k})\}$ is easily obtained as follows:

$$K^{11}(\mathbf{k})=2K_2\cos\mathbf{k}\cdot\mathbf{c}=K^{44}(\mathbf{k}),$$

$$K^{22}(\mathbf{k})=2K_2'\cos\mathbf{k}\cdot\mathbf{c}=K^{33}(\mathbf{k}),$$

$$K^{12}(\mathbf{k})=K_1(1+e^{-i\mathbf{k}\cdot(\mathbf{a}+\mathbf{b})}+e^{-i\mathbf{k}\cdot\mathbf{a}}+e^{-i\mathbf{k}\cdot\mathbf{b}})=K^{21}(-\mathbf{k}),$$

$$K^{13}(\mathbf{k})=K_3(1+e^{-i\mathbf{k}\cdot\mathbf{c}})=K^{31}(-\mathbf{k}),$$

$$K^{14}(\mathbf{k})=0=K^{41}(\mathbf{k}),$$

$$K^{23}(\mathbf{k})=0=K^{32}(\mathbf{k}),$$

$$K^{24}(\mathbf{k})=K^{13}(\mathbf{k}),$$

$$K^{34}(\mathbf{k}) = K^{12}(\mathbf{k}). \tag{B1}$$

We calculate the energy eigenvalues $E^{\sigma}(\mathbf{k})$ and the normal coordinate $\tau^{\sigma}(\mathbf{k})$ using Eq. (8), focusing our attention on the modes belonging to the lowest energy branch λ. Figure 6 gives the calculated contours of the energy eigenvalues $E^{\lambda}(\mathbf{k})$ in the $(0,k,l)_{\mathrm{ortho}}$ plane, which shows that the most stable orbital configuration is given by the orbital wave state defined by the wave vector $\mathbf{k}_0' = (0,0,\frac{1}{2})_{\mathrm{ortho}} = (\frac{1}{2},\frac{1}{2},\frac{1}{4})_{\mathrm{cubic}}$.

The normal coordinate $C^{\lambda}(\mathbf{k}_0')$ corresponding to the lowest energy state is given by solving,

$$[\mathbf{K}(\mathbf{k}_0') - E^{\lambda}(\mathbf{k}_0')\mathbf{1}] \cdot \mathbf{C}^{\lambda}(\mathbf{k}) = 0, \qquad \mathbf{k}_0' = (0,0,\tfrac{1}{2})_{\mathrm{ortho}}. \tag{B2}$$

By substitution of $\{K^{\kappa\kappa'}(\mathbf{k}_0')\}$ and $E^{\lambda}(\mathbf{k}_0')$, it is easily found that

$$C^{\lambda}(\mathbf{k}_0') = \tfrac{1}{2}(1,-1,e^{i\varphi},-e^{i\varphi}), \tag{B3}$$

where $\varphi$ is an arbitrary phase angle. This means that the system is separated into two independent sublattices composed of $\kappa = (1,2)$ and $\kappa = (3,4)$ (see Fig. 8). Each sublattice forms the same ''antiferro'' order while the relative phase relation between the sublattices is left undetermined. This is simply due to that, for the ''antiferro'' order, the orbital configuration on one of the sublattices is frustrated against the other by the translational symmetry of the sublattices.


[1] P. G. Radaelli, D. E. Cox, M. Marezio, S-W. Cheong, P. E. Schiffer, and A. P. Ramirez, Phys. Rev. Lett. **75**, 4488 (1995), and references cited therein.

[2] S-W. Cheong and C. H. Chen, in *Colossal Magnetoresistance, Charge Ordering and Related Properties of Manganese Oxides*, edited by C. N. R. Rao and B. Raveau (World Scientific, Singapore, 1998).

[3] Y. Yamada, O. Hino, S. Nohdo, R. Kanao, T. Inami, and S. Katano, Phys. Rev. Lett. **77**, 904 (1996).

[4] T. Inami, N. Ikeda, Y. Murakami, I. Koyama, Y. Wakabayashi, and Y. Yamada, Jpn. J. Appl. Phys., Suppl. **38-1**, 212 (1999).

[5] A. Urushibara, Y. Moritomo, T. Arima, A. Asamitsu, G. Kido, and Y. Tokura, Phys. Rev. B **51**, 14 103 (1995).

[6] Y. Endoh, K. Hirota, S. Ishihara, S. Okamoto, Y. Murakami, A. Nishizawa, T. Fukuda, H. Kimura, H. Nojiri, K. Kaneko, and S. Maekawa, Phys. Rev. Lett. **82**, 4328 (1999).

[7] S. Katano, Y. Ishii, Y. Morii, H. R. Child, and J. A. Fernandez-Baca, Physica B **241-243**, 198 (1998); Progress Report on JAERI-ORNL Cooperative Neutron Scattering Research, edited by M. Iizumi, JAERI-M **85-112** (1985).

[8] J. D. Lee and B. I. Min, Phys. Rev. B **55**, R14 713 (1997).

[9] S. K. Mishra, R. Pandit, and S. Satpathy, Phys. Rev. B **56**, 2316 (1997).

[10] L. Sheng and C. S. Ting, Phys. Rev. B **57**, 5265 (1998).

[11] S. Mori, C. H. Chen, and S-W. Cheong, Phys. Rev. Lett. **81**, 3972 (1998).

[12] S. Mori, T. Katsufuji, N. Yamamoto, C. H. Chen, and S-W. Cheong, Phys. Rev. B **59**, 13 573 (1999).

[13] N. Fukumoto, S. Mori, N. Yamamoto, and Y. Moritomo (private communication).

[14] P. B. Allen and V. Perebeinos, Phys. Rev. B **60**, 10 747 (1999).

[15] S. Ishihara, J. Inoue, and S. Maekawa, Phys. Rev. B **55**, 8280 (1997).